BIOCHEMISTRY
including biophysical chemistry & molecular biology

Article

pubs.acs.org/biochemistry

Divergent Evolution of Ligand Binding in the *o*-Succinylbenzoate Synthase Family

Denis Odokonyero,[†] Sugadev Ragumani,[‡] Mariana S. Lopez,[†] Jeffrey B. Bonanno,[∥] Nicole D. S. Ozerova,[†] DaNae R. Woodard,[†] Benjamin W. Machala,[†] Subramanyam Swaminathan,[‡] Stephen K. Burley,[§] Steven C. Almo,[∥,⊥] and Margaret E. Glasner*[,†]

[†]Department of Biochemistry and Biophysics, Texas A&M University, 2128 TAMU, College Station, Texas 77843-2128, United States

[‡]Biosciences Department, Brookhaven National Laboratory, Upton, New York 11973, United States

[§]Center for Integrative Proteomics Research, Rutgers Cancer Institute of New Jersey, Research Collaboratory for Structural Bioinformatics Protein Data Bank, and Department of Chemistry and Chemical Biology, Rutgers, The State University of New Jersey, 174 Frelinghuysen Road, Piscataway, New Jersey 08854-8076, United States

[∥]Department of Biochemistry and [⊥]Department of Physiology and Biophysics, Albert Einstein College of Medicine, 1300 Morris Park Avenue, Bronx, New York 10461, United States

Supporting Information

ABSTRACT: *Thermobifida fusca o*-succinylbenzoate synthase (OSBS), a member of the enolase superfamily that catalyzes a step in menaquinone biosynthesis, has an amino acid sequence that is 22 and 28% identical with those of two previously characterized OSBS enzymes from *Escherichia coli* and *Amycolatopsis* sp. T-1-60, respectively. These values are considerably lower than typical levels of sequence identity among homologous proteins that have the same function. To determine how such divergent enzymes catalyze the same reaction, we determined the structure of *T. fusca* OSBS and identified amino acids that are important for ligand binding. We discovered significant differences in structure and conformational flexibility between *T. fusca* OSBS and other members of the enolase superfamily. In particular, the 20s loop, a flexible loop in the active site that permits ligand binding and release in most enolase superfamily proteins, has a four-amino acid deletion and is well-ordered in *T. fusca* OSBS. Instead, the flexibility of a different region allows the substrate to enter from the other side of the active site. *T. fusca* OSBS was more tolerant of mutations at residues that were critical for activity in *E. coli* OSBS. Also, replacing active site amino acids found in one protein with the amino acids that occur at the same place in the other protein reduces the catalytic efficiency. Thus, the extraordinary divergence between these proteins does not appear to reflect a higher tolerance of mutations. Instead, large deletions outside the active site were accompanied by alteration of active site size and electrostatic interactions, resulting in small but significant differences in ligand binding.

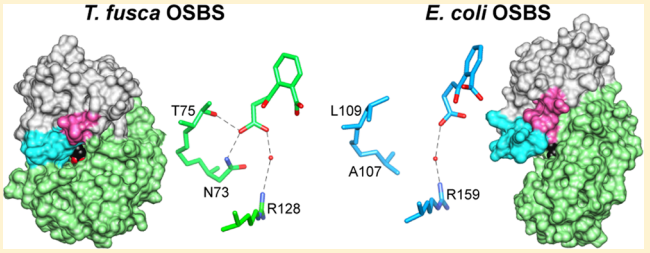

Understanding the natural diversity of enzyme superfamilies is critical for improving functional annotation and protein engineering methods. Toward this end, the enolase superfamily has been extensively studied. Enzymes in the enolase superfamily catalyze more than 20 chemical reactions.[1,2] All of these reactions involve the abstraction of a proton from the α-carbon of a carboxylate and stabilization of the enolate anion intermediate by a divalent cation. The conserved catalytic residues are in a $(\beta/\alpha)_7$ β-barrel, which is connected to an $\alpha + \beta$ fold domain that forms a cap over the active site. Several recent studies used homology models and computational ligand docking to accurately predict specificity in the dipeptide epimerase family, a family in the enolase superfamily.[3−5] Extending this approach to the rest of the enolase superfamily requires experimental determination of a representative set of structures in the superfamily to serve as templates for homology models. In addition, characterizing the structural plasticity of proteins in the enolase superfamily offers valuable insight into the designability of the enolase superfamily fold.

Here, we analyze structure−function relationships of *Thermobifida fusca o*-succinylbenzoate synthase (OSBS), a member of the enolase superfamily. This protein belongs to the large, extremely divergent OSBS family. The biological function of most enzymes in the OSBS family is OSB synthesis, which is a step in menaquinone (vitamin K) biosynthesis. However, some enzymes in one branch of the family (the NSAR/OSBS subfamily) also catalyze *N*-succinylamino acid racemization [NSAR (Figure 1)].[6−8] Members of two subfamilies,

Received: August 27, 2013
Published: September 24, 2013

   dx.doi.org/10.1021/bi401176d | *Biochemistry* 2013, 52, 7512−7521

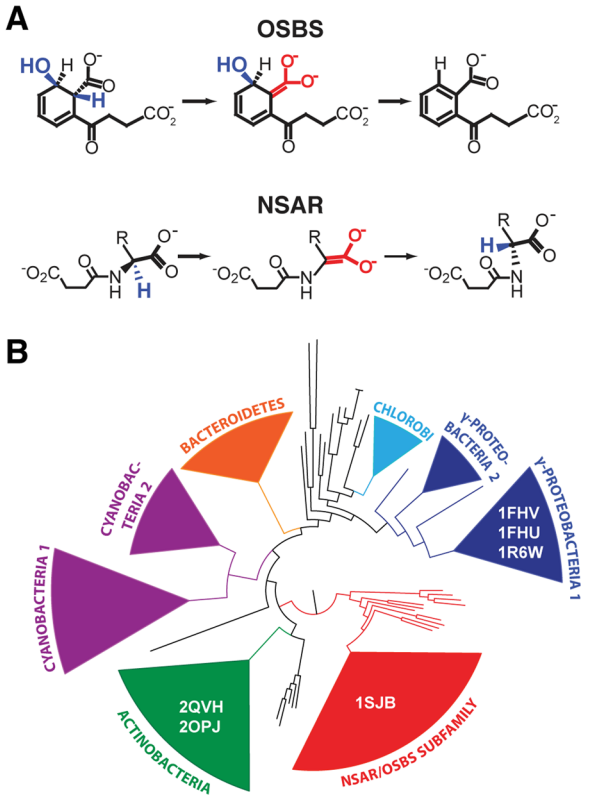

Figure 1. OSBS family. (A) *o*-Succinylbenzoate synthase (OSBS) and *N*-succinylamino acid racemase (NSAR) reactions. The enolate anion intermediate that occurs in all reactions in the enolase superfamily is colored red; blue atoms are lost or rearranged in the reactions. R represents the hydrophobic amino acid side chain. (B) Phylogenetic tree showing the division of the OSBS family into eight major subfamilies.[14] The structure of *T. fusca* OSBS (PDB entries 2OPJ and 2QVH) from the Actinobacteria subfamily is reported in this work. It is compared to *E. coli* OSBS (PDB entries 1FHV, 1FHU, and 1R6W) from the γ-Proteobacteria 1 subfamily and *Amycolatopsis* NSAR/OSBS (PDB entry 1SJB) from the NSAR/OSBS subfamily.

Escherichia coli OSBS from the γ-Proteobacteria 1 subfamily and *Amycolatopsis* NSAR/OSBS from the NSAR/OSBS subfamily, were previously characterized.[9−14] *T. fusca* OSBS belongs to the Actinobacteria OSBS subfamily. Like the γ-Proteobacteria 1 subfamily, genome context indicates that OSBS is the biological function of all members of the Actinobacteria subfamily.[6,7] The amino acid sequence of *T. fusca* OSBS is 22% and 28% identical with those of *E. coli* OSBS and *Amycolatopsis* NSAR/OSBS, respectively. These values are considerably lower than typical levels of sequence identity among homologous proteins whose functions are conserved.[15,16] This could indicate that members of the OSBS family are more tolerant of mutations than typical proteins. To understand how such divergent enzymes catalyze the same reaction, we determined the structure of *T. fusca* OSBS and identified amino acids that are important for ligand binding.

Our experiments identified significant differences in structure and conformational flexibility between *T. fusca* OSBS and other members of the enolase superfamily. In particular, the 20s loop, which is a flexible loop from the capping domain that permits ligand binding and release in most enolase superfamily proteins, has a four-amino acid deletion and is well-ordered in *T. fusca* OSBS. Instead, the conformational flexibility of a different region allows the substrate to enter from the other side of the active site. Our results also show that *T. fusca* OSBS was more tolerant of mutations at residues that were critical for activity in *E. coli* OSBS, even though their molecular functions are conserved.[14] Replacing active site amino acids found in one of the proteins with the amino acids that occur at the same place in the other protein reduces catalytic efficiency. Thus, the extraordinary divergence between these proteins does not appear to reflect a heightened ability to tolerate mutations. Instead, the rate of divergence in the OSBS family appears to be dominated by large deletions in the capping domain and loss of quaternary structure (D. Odokonyero et al., manuscript in preparation). These structural changes occurred along with alteration of active site size and electrostatic interactions, resulting in small but significant differences in ligand binding.

MATERIALS AND METHODS

Protein Production and Crystallization. The target gene for Tfu_1410 from *T. fusca* (encoding amino acids 2−317) was obtained via synthesis (Codon Devices), amplified via polymerase chain reaction (PCR), cloned into a C-terminal His_6-tag expression vector, tested for expression and solubility, fermented on a large scale, purified, and crystallized using the published methods employed by the NYSGXRC.[17] Detailed protocols for the effort on this target are publicly available from the NIGMS PSI repository of publicly available protocols, TargetTrack (http://sbkb.org/tt/index.html), by searching on "Project Target ID" NYSGXRC-9312b; the expression clone is available from the PSI Materials Repository (http://dnasu.asu.edu/DNASU/GetCloneDetail.do?cloneid=336395).

Se-Met-labeled material was generated by a 1 L fermentation of HY medium (Medicilon, Inc.) yielding 43 mg of purified protein. The purity and Se incorporation were confirmed by sodium dodecyl sulfate−polyacrylamide gel electrophoresis (SDS−PAGE) analysis of chromatographic fractions and mass spectrometry (electrospray ionization and matrix-assisted laser desorption ionization) of the final pool. This sample was used for structure determination of the apo and liganded forms of this protein.

Diffraction-quality single crystals of the apo form were obtained by mixing 1 μL of protein at a concentration of 20 mg/mL with 1 μL of 100 mM Bis-Tris (pH 5.5), 25% polyethylene glycol (PEG) 3350, and 200 mM ammonium acetate and equilibrating by vapor diffusion against 100 μL of the same precipitant at room temperature. Crystals of the complex were obtained with a similar procedure using a well solution of 0.1 M Bis-Tris (pH 6.5), 25% PEG 3350, 0.2 M ammonium acetate, 10 mM magnesium chloride, and 10 mM *o*-succinylbenzoate. The resulting crystals were cryoprotected and flash-frozen in liquid nitrogen.

Collection of Data for and Determination of the Structure of Apo OSBS. Single-wavelength anomalous diffraction data from apo crystals, consistent with space group *P*1 and extending to 1.6 Å resolution, were collected in the vicinity of the selenium anomalous peak wavelength (λ = 0.9795 Å) at the Brookhaven National Laboratory National Synchrotron Light Source X12C beamline. Matthews coefficient calculations were consistent with the presence of one molecule in the asymmetric unit (ASU).

Two selenium sites were located using SHELXD,[18] and density-modified SAD phases were calculated with SHARP[19] and SOLOMON.[20] Following several rounds of automated and manual model building using CCP4[21] and Coot,[22] respectively,

dx.doi.org/10.1021/bi401176d | *Biochemistry* 2013, 52, 7512−7521

refinement using CNS[23] converged at an R_{work} of 20.2% and an R_{free} of 22.6%.

The final model consists of one chain of *T. fusca* Tfu_1410 (2215 protein atoms; Thr2−Gln310), 201 waters, and the N-terminal SL cloning artifact. Several segments [Arg101−Ala106, Asp177−Leu187, Val311−Pro317, and the C-terminal cloning artifact (EGHHHHHH)] were not observed in the electron density presumably because of disorder, consistent with modest flexibility. The coordinates and structure factors have been deposited in the Protein Data Bank as entry 2OPJ.

Collection of Data for and Determination of the Structure of the OSBS−Product Complex. Diffraction data from complex crystals, consistent with space group *P*1 [albeit with a cell and ASU different from those of the apo form (see Table 1)] and extending to 1.76 Å resolution, were collected in the vicinity of the selenium anomalous peak wavelength (λ = 0.9795 Å) at the Brookhaven National Laboratory National Synchrotron Light Source X29A beamline. Matthews coefficient calculations were consistent with the presence of two molecules in the ASU.

Two copies of the protein were placed via molecular replacement using MOLREP.[24] The model was rebuilt using CCP4[21] and Coot.[22] Coordinated Mg^{2+} ions and *o*-succinylbenzoate molecules were placed unambiguously prior to the final stages of refinement based on clear features in the difference Fourier synthesis electron density maps. Refinement using CNS[23] converged at an R_{work} of 21.8% and an R_{free} of 25.1%.

The final model consists of two chains of *T. fusca* Tfu_1410 (4698 protein atoms; chains A and B, Thr2−Gln310), two magnesium ions, two *o*-succinylbenzoate molecules, 286 waters, and both N-terminal SL cloning artifacts. The C-terminal segments [Val311−Pro317 and the C-terminal cloning artifact (EGHHHHHH)] were not observed in the electron density presumably because of disorder, consistent with modest flexibility. The coordinates and structure factors have been deposited in the Protein Data Bank as entry 2QVH.

Table 1. Crystallographic Data Collection and Refinement Statistics for 2OPJ and 2QVH[a]

	apo	product-bound
	Data Collection	
PDB entry	2OPJ	2QVH
space group	*P*1	*P*1
cell dimensions	*a* = 36.976 Å	*a* = 44.543 Å
	b = 37.642 Å	*b* = 52.877 Å
	c = 51.990 Å	*c* = 61.449 Å
	α = 71.28°	α = 70.53°
	β = 76.13°	β = 87.22°
	γ = 73.23°	γ = 85.56°
no. of molecules per ASU	1	2
wavelength (Å)	0.9795	0.9795
resolution (Å)	50−1.60 (1.66−1.60)	50.0−1.76 (1.82−1.76)
no. of unique reflections	29912	48053
completeness (%)	90.5 (52.7)	92.0 (95.2)
R_{sym} (%)	0.037 (0.108)	0.042 (0.092)
$\langle I/I \rangle$	11.3 (2.0)	23.2 (2.0)
redundancy	3.9 (3.6)	3.8 (3.7)
	Refinement	
R/R_{free}	20.2/22.6	21.8/25.1
no. of atoms		
protein	2215	4698
solvent	201	286
ligand	NA	34
average *B* factor (Å^2)		
protein	12.8	19.1
solvent	22.9	24.1
ligand	NA	14.6
Ramachandran statistics (%)		
favored	94.0	92.2
allowed	6.0	7.9
outlier	0	0
root-mean-square deviation from ideal		
bonds (Å)	0.005	0.005
angles (deg)	1.30	1.20

[a]Values in parentheses are for the highest-resolution shell. NA, not applicable.

Structural Alignments. The structures of *T. fusca* OSBS were aligned with those of *E. coli* OSBS and *Amycolatopsis* NSAR/OSBS using the structure matching and alignment tools in UCSF Chimera (Resource for Biocomputing, Visualization, and Informatics at the University of California, San Francisco, supported by National Institute of General Medical Sciences Grant P41-GM103311).[25] The alignment was manually refined on the basis of visual inspection of the structural alignment.

Mutagenesis. Site-directed mutagenesis was performed by the QuikChange Mutagenesis protocol using a two-stage PCR (see the Supporting Information for primers and PCR conditions).[26] The templates for mutagenesis were the *menC* gene from *E. coli* (gi number 16130196) subcloned into a modified pET15b vector (Novagen) with a 10-histidine N-terminal tag and *T. fusca* OSBS, which was subcloned into pET15b. Mutations were confirmed by sequencing in both directions (Eton Bioscience, Inc.).

Protein Purification for Enzymatic Assays. All proteins were expressed in *menC*$^-$ strain BW25113 (*menC::kan*, DE3) to ensure that the purified proteins would not be contaminated with wild-type OSBS.[14] Cultures were grown overnight at 37 °C without induction in Luria-Bertani broth supplemented with carbenicillin and kanamycin. Cells were harvested by centrifugation and resuspended in buffer containing 20 mM Tris (pH 8.0), 500 mM NaCl, 5 mM imidazole, 0.02 mg/mL DNase (Worthington), and 2 μM phenylmethanesulfonyl fluoride (PMSF) (Thermo Scientific). Resuspended pellets were lysed by sonication. After centrifugation, the filtered lysate was applied to a 5 mL HisTrap FF column charged with Ni^{2+} (GE Healthcare). The protein was eluted with a buffer containing 20 mM Tris (pH 8.0), 500 mM NaCl, and 500 mM imidazole using a step to 15% elution buffer followed by a linear gradient to 100% elution buffer. Fractions containing apparently homogeneous protein were identified by SDS−PAGE and pooled. Amicon Ultra-15 centrifugal filters (10 kDa cutoff) (Millipore) were used to exchange the buffer and concentrate the pooled fractions. Purified proteins were stored in 10 mM Tris (pH 8.0) and 5 mM $MgCl_2$ supplemented with 25% glycerol for storage at −80 °C.

OSBS Activity Assay. Wild-type and mutant OSBS enzymes were assayed with varying concentrations of 2-succinyl-6-hydroxy-2,4-cyclohexadiene-1-carboxylate (SHCHC) in 50 mM Tris (pH 8.0) and 0.1 mM $MnCl_2$ at 25 °C. SHCHC was synthesized as described previously.[9,14] The

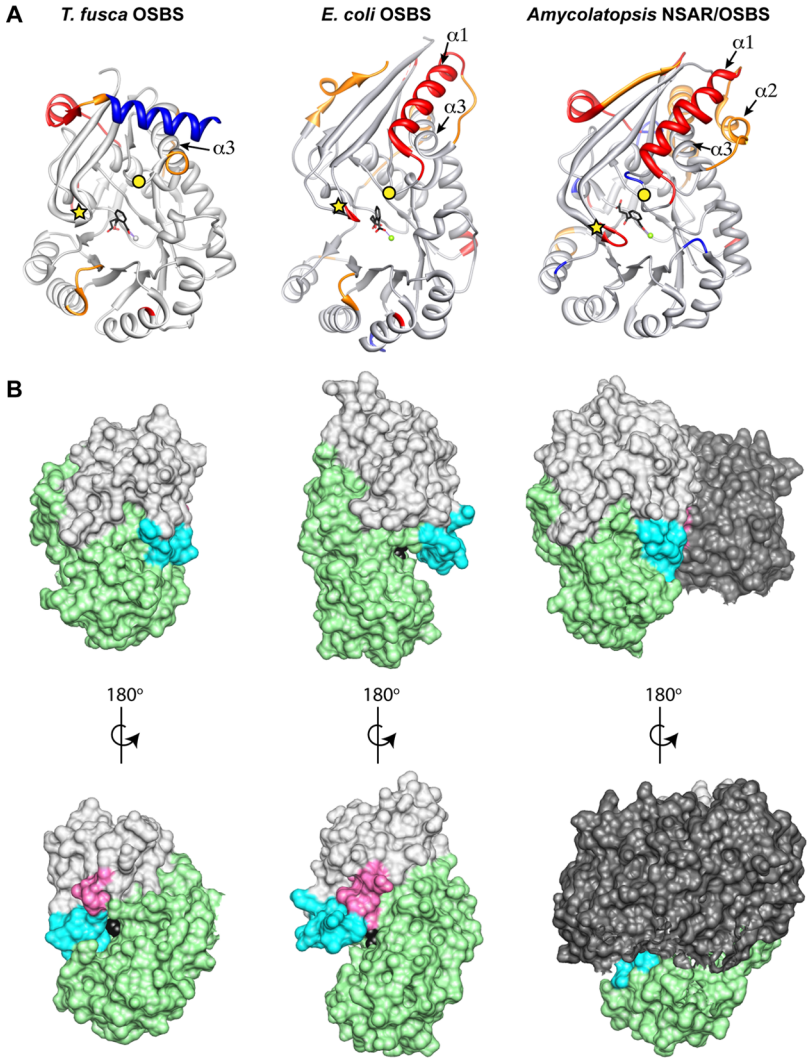

Figure 2. Comparison of OSBS enzymes from *T. fusca* (PDB entry 2QVH), *E. coli* (PDB entry 1FHV), and *Amycolatopsis* sp. T-1-60 (PDB entry 1SJB).[11,13] (A) Insertions and deletions. Regions colored red are deleted in one of the other enzymes. Regions colored blue are insertions in that enzyme. Regions icolored orange have insertions and deletions in all three enzymes and cannot be aligned with each other. OSB is colored black, and the magnesium ion is colored lime green. The 20s loops and 50s loops are marked with a star and a circle, respectively. The three α-helices of the capping domain are labeled. (B) Active site accessibility. Space-filling models have been rotated 90° toward the right (top) or left (bottom) relative to panel A. The 20s loop is colored cyan, the 50s loop pink, the rest of the capping domain light gray, and the barrel domain green. Another subunit of the *Amycolatopsis* NSAR/OSBS octamer is colored dark gray to illustrate subunit interactions. OSB is colored black.

assays were performed by quantifying the decrease in absorbance at 310 nm ($\Delta = -2400\ M^{-1}\ cm^{-1}$), as previously described.[9,10] Initial rates were calculated using VisionPro (Thermo Scientific) and fit to the Michaelis–Menten equation using Kaleidagraph (Synergy Software).

RESULTS

Structure of *T. fusca* OSBS. The structure of *T. fusca* OSBS exhibits some unexpected differences from those of other members of the enolase superfamily. Like *E. coli* OSBS, it is monomeric, which is atypical in the enolase superfamily (D. Odokonyero et al., manuscript in preparation). *T. fusca* and *E. coli* OSBSs are ~40 amino acids shorter than average enolase superfamily members, at 319 and 320 amino acids, respectively, although deletions occur at different sites (Figure 2A; D. Odokonyero et al., manuscript in preparation). Surprisingly, *T. fusca* OSBS has a four-amino acid deletion in the 20s loop, which is around position 20 in the capping domain. In other members of the enolase superfamily, the 20s loop helps close the active site when substrate or product is bound.[11,27−30] In *Amycolatopsis* NSAR/OSBS, the 20s loop completely closes the active site (Figure 2B).[13] However, the active site is partially open in both *T. fusca* and *E. coli* OSBSs.[11] In *T. fusca* OSBS, the 20s loop closes one side of the active site by contacting the barrel domain, but there is an opening on the other side of the active site because of the deletion. In contrast, the active site in *E. coli* OSBS is a deep, open crevice because the 20s loop does not contact the barrel domain.[11]

The other unexpected finding was that the first two helices of the capping domain, which are found in almost all other members of the enolase superfamily, have been deleted in *T. fusca* OSBS. The deletion begins after the second active site loop (the 50s loop), where the chain takes a short-cut to α-helix 3 of the capping domain. This deletion is conserved in all members of the Actinobacteria subfamily. The second α-helix of the capping domain is also truncated or deleted in *E. coli* and many other OSBSs (D. Odokonyero et al., manuscript in preparation). These helices are not in the active site, but they

dx.doi.org/10.1021/bi401176d | *Biochemistry* 2013, 52, 7512−7521

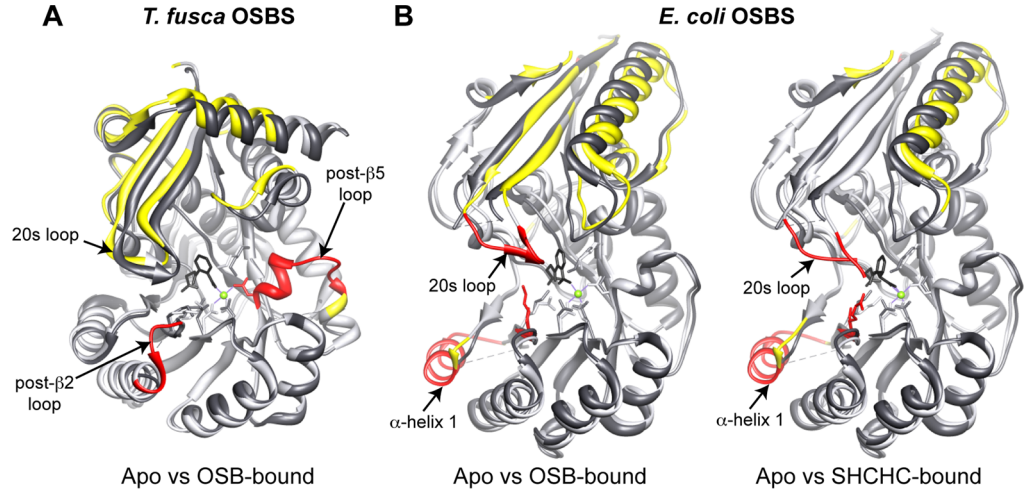

Figure 3. Comparison of changes in conformation upon ligand binding. Apo and ligand-bound structures were aligned by superimposing the conserved catalytic motifs in the barrel domain. The apo structure is colored dark gray and the ligand-bound structure light gray. Regions that become ordered upon ligand binding are colored red, and residues whose α-carbons shift by >2 Å are colored yellow. (A) *T. fusca* OSBS in the presence and absence of OSB (PDB entries 2QVH and 2OPJ, respectively). (B) *E. coli* OSBS in the absence (PDB entry 1FHU) and presence of OSB (PDB entry 1FHV) or SHCHC (PDB entry 1R6W).[11,12]

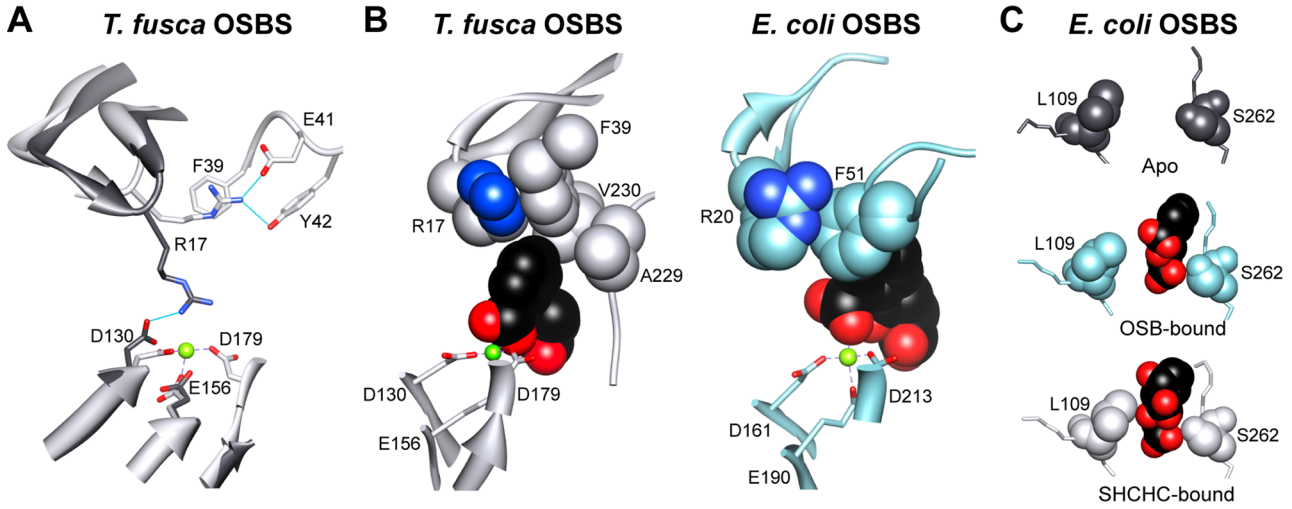

Figure 4. Changes in conformation in the active site. (A) In *T. fusca* OSBS, R17 forms a salt bridge with one of the metal-binding residues in the absence of OSB and Mg^{2+} (dark gray, PDB entry 2OPJ). When OSB and Mg^{2+} are bound, R17 interacts with three residues from the 50s loop instead (light gray, PDB entry 2QVH). (B) In *T. fusca* OSBS bound to OSB (gray, PDB entry 2QVH), R17, F39, V230, and A229 form a pocket for binding the top of OSB (black). The structure is rotated ~90° toward the left relative to panel A. In *E. coli* OSBS bound to OSB (PDB entry 1FHV), the 20s and 50s loops interact via R20 and F51. The Mg^{2+} ion is shown as a lime sphere. (C) In *E. coli* OSBS, L109 and S262 form a slot where the succinyl tail of the substrate and product bind. The apo structure (PDB entry 1FHU) is colored dark gray, the product-bound structure light blue (PDB entry 1FHV), and the substrate-bound structure light gray (PDB entry 1R6W).[11,12] OSB and HCHC are colored black.

are at the interface between subunits in the octameric *Amycolatopsis* NSAR/OSBS and most other multimeric enolase superfamily members.[13,30−36] *T. fusca* OSBS appears to compensate for the loss of these helices with an extra helix appended to the C-terminus that crosses over the top of the capping domain. This helix is not present in any other enolase superfamily members.

Changes in Conformation between Apo and Product-Bound Forms. In most structurally characterized enolase superfamily proteins, including *E. coli* OSBS, the 20s loop is disordered in the absence of substrate or product.[11,27−30,37] Although the 20s loop helps determine specificity by making hydrogen bonds with the substrate in some enolase superfamily members,[5,30] substitutions and deletions in the 20s loop of *E. coli* OSBS and *Pseudomonas putida* mandelate racemase suggest that it serves primarily as a "flexible flap" that partially closes the active site to limit substrate dissociation.[14,38]

In contrast, the 20s loop of *T. fusca* OSBS is ordered in the presence and absence of bound OSB. Instead, two other regions are disordered in the apo structure. The first is the loop after β-strand 2 in the barrel domain (post-β2), which has a four-amino acid insertion (Figure 3). This insertion is present only in the Actinobacteria OSBS subfamily. When product is bound, some atoms of post-β2 are within 5 Å of the 20s loop, but there are no hydrogen bonds between the highly polar post-β2 loop (sequence of ERGQSEA) and the 20s loop. Post-β2 is also >13 Å from the deeply buried substrate. While it might help restrict entrance or exit of the ligand from its position at the mouth of the active site, its distance from the 20s loop and OSB suggests that post-β2 becomes ordered

dx.doi.org/10.1021/bi401176d | *Biochemistry* 2013, 52, 7512−7521

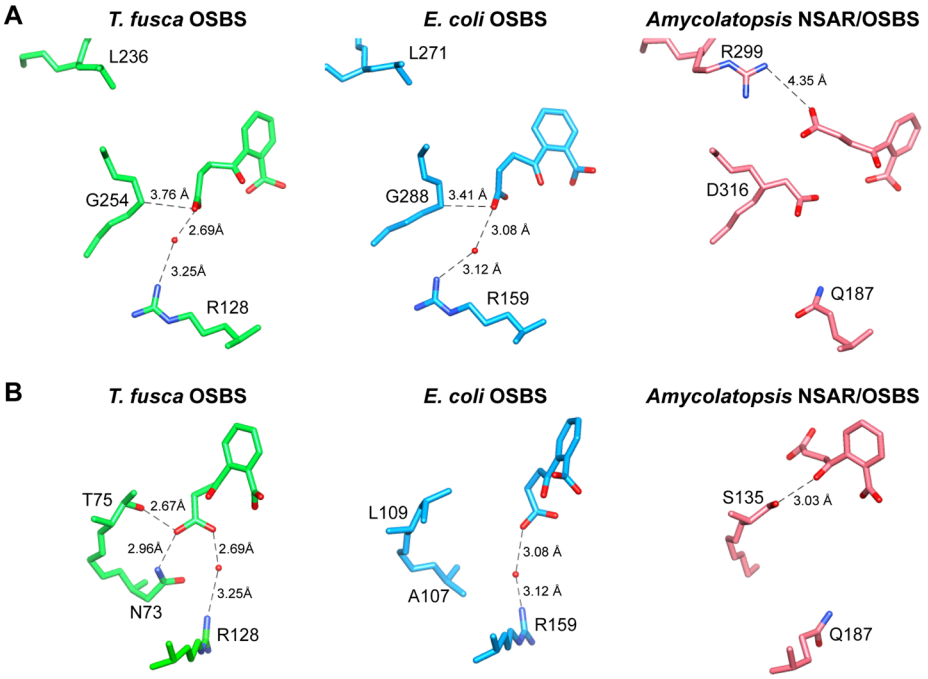

Figure 5. Comparison of ligand contacts in the active site. (A) Position of the ligand relative to R128, L236, and G254 of *T. fusca* OSBS and related enzymes.[11,12] (B) Interaction between the ligand and β-strand 1 of the barrel domain. The images are rotated ~90° toward the left relative to panel A, so that L236 and G254 would be behind the ligand.

because of greater overall protein stability when ligand is bound, as observed in other proteins.[39,40]

The second region that becomes ordered when OSB is bound is a loop following β-strand 5 (post-β5) in the barrel domain. One of the metal-binding residues is in this loop. No metal ion is bound to the apoprotein because magnesium chloride was not present in the crystallization conditions. However, flexibility of this loop is probably not a crystallization artifact, because in the structure bound to OSB and Mg^{2+}, B-factors of atoms in residues 184−190 of this loop are in the top 10%. Ordering this loop causes a small change in conformation that propagates through the capping domain. When product is bound, post-β5 collides with the 50s loop. Because the 50s loop contacts the 20s loop and the C-terminal helix that crosses over the top of the capping domain, they also move ≥2 Å toward the left in Figure 3A. Consequently, ordering the post-β5 loop does not completely close the entrance to the active site. Nevertheless, partial occlusion of the active site by post-β5 only when ligand is bound suggests that post-β5, instead of the 20s loop, provides an entry portal for substrate binding. Thus, ordering this loop assists catalysis by forming the metal-binding site and sterically limiting substrate dissociation.

In addition to these large-scale movements, the side chain of R17, a residue in the 20s loop, moves 5.1 Å between the apo and product-bound forms of *T. fusca* OSBS. R17 moves from the center of the active site where it interacts with one of the Mg^{2+}-binding residues in the apo structure to a cation−π interaction with F39 in the 50s loop of the capping domain when OSB binds. From this position, it can also form a salt bridge with E41 and a hydrogen bond with Y42 (Figure 4A). R17, F39, E41, and Y42 are conserved in nearly all members of the Actinobacteria subfamily.[14] The δ-carbons of R17, F39, A229, and V230 form a hydrophobic pocket for the cyclohexyl ring of the substrate (Figure 4B).

We compared apo and ligand-bound structures of *T. fusca* OSBS to structures of *E. coli* OSBS, which has also been determined in the apo and product-bound forms.[11] In addition, a substrate-bound enzyme was determined by mutating the catalytic lysine (K133) to arginine.[12] Two regions of *E. coli* OSBS undergo disorder−order transitions upon ligand binding, the 20s loop and the first α-helix of the barrel. When substrate or product is bound, the 20s loop and connected β-strands in the capping domain rotate backward in Figure 3B. The ordered 20s loop collides with the 50s loop, rotating it and the following helices backward and to the right, in the opposite direction of the change in conformation in *T. fusca* OSBS.

In *E. coli* OSBS, structural transitions of the first α-helix of the barrel are associated with β-strand 1 of the barrel moving slightly closer to β-strand 7 on the opposite side of the barrel (Figure 4C). Two residues on these strands, L109 and S262, form a slot where the succinyl tail of the substrate and product bind. The distance is widest in the product-bound structure, with 9.8 Å between the δ-carbon of L109 and the hydroxyl of S262. This distance shrinks to 8.5 Å when substrate binds. Although mutating S262 to glycine had little effect, mutating L109 to alanine reduced the efficiency 24-fold.[14] Together, the structural and mutational data suggest that small movements of β-strand 1 could be important for substrate binding and product release.

In summary, the changes in conformation between apo and ligand-bound structures of *T. fusca* OSBS and *E. coli* OSBS are different. *E. coli* OSBS is more similar to other members of the enolase superfamily, in that flexibility of the 20s loop allows ligand binding and release.[11,27−30,37] This is accompanied by the flexibility of the first α-helix and β-strand of the barrel. In contrast, both the 20s loop and first β-strand of the barrel are well-structured in the apo and product-bound forms of *T. fusca* OSBS. Instead, a deletion in the 20s loop and a disordered region in the post-β5 loop suggest that substrate binding and

dx.doi.org/10.1021/bi401176d | *Biochemistry* 2013, 52, 7512−7521

Table 2. Effects of Mutations on OSBS Activity[a]

variant	k_{cat} (s^{-1})	K_M (μM)	k_{cat}/K_M (M^{-1} s^{-1})	relative k_{cat}/K_M	variant	k_{cat} (s^{-1})	K_M (μM)	k_{cat}/K_M (M^{-1} s^{-1})	relative k_{cat}/K_M
T. fusca OSBS					*E. coli* OSBS				
WT	122 ± 4.6	182 ± 22	6.7×10^5	1.0	WT[b]	24 ± 0.8	12 ± 1.8	2.0×10^6	1.0
20s del[c]	0.1 ± 0.005	54 ± 8	1.9×10^3	0.003	20s del[b,d]	0.2 ± 0.003	29 ± 1.3	6.9×10^3	0.0034
F16A	4.4 ± 1	36 ± 1	1.2×10^5	0.18	L19A[b]	3.9 ± 0.1	13 ± 2.4	3.0×10^5	0.15
R17A	0.6 ± 0.02	7 ± 1.4	8.6×10^4	0.13	R20S	0.5 ± 0.1	22 ± 0.1	2.3×10^4	0.01
F39A	163 ± 19	666 ± 151	2.5×10^5	0.37	L48A[b]	14 ± 0.8	111 ± 17	1.3×10^5	0.063
Y42A	210 ± 13	588 ± 74	3.6×10^5	0.5	F51A[b]	49 ± 2.6	122 ± 21	4.0×10^5	0.20
R17A/F39A	0.2 ± 0.01	48 ± 6	4.2×10^3	0.006					
R17A/Y42A	0.36 ± 0.01	38 ± 4.2	9.5×10^3	0.014	R20S/F51A	0.616 ± 0.03	144 ± 19	4.3×10^3	0.002
N73A	10 ± 0.7	322 ± 56	3.1×10^4	0.05	A107N	32 ± 1.9	109 ± 17	2.9×10^5	0.13
T75A	55 ± 1.5	154 ± 15	3.6×10^5	0.53	L109A[b]	2.9 ± 0.2	36 ± 8	8.0×10^4	0.042
T75L	18 ± 0.5	57 ± 5	3.2×10^5	0.47	L109T	3.6 ± 0.3	83 ± 17	4.3×10^4	0.022
					L109S	5.8 ± 0.2	78 ± 9	7.4×10^4	0.037
N73A/T75A	na[e]	na[e]	na[e]	na[e]					
N73L/T75V	0.18 ± 0.01	300 ± 63	6.1×10^2	0.0009					
N73A/T75L	5.1 ± 0.4	256 ± 51	2.0×10^4	0.03	A107N/L109T	2.4 ± 0.2	456 ± 85	5.3×10^3	0.0026
R128M	104 ± 4	470 ± 42	2.2×10^5	0.33	R159M[b]	0.9 ± 0.05	80 ± 15	1.1×10^4	0.0056
G254A	16 ± 0.3	86 ± 6	1.9×10^5	0.28	G288A[b]	nd[f]	nd[f]	3.8×10^3	0.0019
G254T	13 ± 0.7	668 ± 72	1.9×10^4	0.03					
V230L	29 ± 1.6	145 ± 22	2.0×10^5	0.30	I265A[b]	6 ± 0.2	10 ± 1.5	5.8×10^5	0.30
Th. elongatus OSBS									
WT	80 ± 4	78 ± 17	1.0×10^6	1.0					
G295A[g]	4 ± 0.4	304 ± 82	1.3×10^4	0.013					

[a]Mutations in the same row are located at the same positions in the structures of the two proteins. [b]From ref 14. [c]The 20s loop in *T. fusca* OSBS was truncated by replacing residues R15, F16, R17, G18, and I19 with glycine. [d]The 20s loop in *E. coli* OSBS was truncated by deleting residues V17, V18, L19, R20, D21, R22, R23, and L24. [e]No activity detected. [f]Not determined because substrate saturation could not be achieved. [g]At the same position in the structure as G288 in *E. coli* OSBS and G254 in *T fusca* OSBS.

product release occur on the opposite side of the active site. This is especially noteworthy because this side of the active site is at the interface between subunits in *Amycolatopsis* NSAR/OSBS and most other multimeric enolase superfamily members.[13,30−36]

Comparison of Ligand Binding. The product OSB binds *E. coli* OSBS and *Amycolatopsis* NSAR/OSBS in different conformations (Figure 5).[11,13] In *E. coli* OSBS, mutating either G288 or R159 interferes with substrate binding in the correct conformation, decreasing catalytic efficiency >200-fold.[14] Except for members of the NSAR/OSBS subfamily, glycine and arginine are conserved at these positions in most other OSBSs, suggesting that most members of the OSBS family bind OSB in the same conformation as *E. coli* OSBS. Consistent with this idea, mutating this glycine (G295A) in *Thermosynechococcus elongatus* OSBS, a member of the Cyanobacteria 1 subfamily, reduces the enzyme's efficiency ∼100-fold.

As predicted, *T. fusca* OSBS binds OSB in the same conformation as *E. coli* OSBS (Figure 5A). However, mutating the conserved glycine (G254A) or arginine (R128M) in *T. fusca* OSBS reduces its catalytic efficiency only ∼3-fold (Table 2). Replacing G254 with threonine had a larger effect, reducing the catalytic efficiency 34-fold. In both enzymes, replacing this glycine with larger amino acids should create a steric conflict with the substrate. According to the CASTp database, the active site volume of *T. fusca* OSBS (1441 Å^3) is larger than that of *E. coli* (1223 Å^3), which might permit the substrate to change its position in the G254A or G254T mutant.[41] However, differences in the calculated active site volumes could be due to differences in determining the boundaries of the binding pocket in these relatively open active sites. Alternatively, *T. fusca* OSBS could be more tolerant of these mutations because of compensation by other protein−ligand interactions [such as the first β-strand in the barrel (see below)], mechanistic differences between the enzymes, or higher stability.

Stronger interactions between the ligand and β-strand 1 in the barrel might help *T. fusca* OSBS tolerate the G254 and R128 mutations. N73 and T75 form hydrogen bonds with the succinyl carboxylate in *T. fusca* OSBS, while A107 and L109 are at the corresponding positions in *E. coli* OSBS (Figure 5B). Mutating T75 to alanine had little effect on catalytic efficiency, but changing N73 to alanine reduced efficiency 20-fold. The N73A/T75A double mutation had no detectable activity. The level of soluble protein expression of this mutant was severely reduced, suggesting that these mutations decrease protein stability. Consequently, we constructed an N73L/T75V variant that retained the shape of the amino acids and yielded the same amount of soluble protein as the wild type. This mutation reduced efficiency 1000-fold. In contrast, replacing N73 and T75 with the residues found in *E. coli* OSBS, alanine and leucine, respectively, reduced activity only 33-fold. Thus, N73 and T75 together make important interactions with the succinyl carboxylate. Loss of these hydrogen bonds can be partially tolerated if the residues are mutated to amino acids found in a related OSBS.

In *E. coli* OSBS, mutating L109 to alanine, serine, or threonine reduced efficiency 24−45-fold. Mutating A107, which is >5 Å from the ligand, to asparagine reduced efficiency only 10-fold. The effect of the A107N/L109T double mutation was additive, reducing efficiency 385-fold. Together, mutations in *E. coli* and *T. fusca* OSBSs demonstrate that amino acids on β-strand 1 make significant contributions to the reaction, and the amino acids are not interchangeable between different OSBSs.

dx.doi.org/10.1021/bi401176d | *Biochemistry* 2013, 52, 7512−7521

Given that its truncated 20s loop is an unusual feature of *T. fusca* OSBS, we also constructed mutations to assess its role in catalysis. Deleting five additional residues to remove the rest of the loop reduced efficiency 300-fold, identical to the effect of deleting the 20s loop in *E. coli* OSBS.[14] Likewise, mutating individual residues that are closest to the ligand (F16 and R17 in *T. fusca* OSBS and L19 in *E. coli* OSBS) reduced efficiency <10-fold. As noted above, R17 interacts with F39 and Y42 in the 50s loop when OSB is bound. Mutating either F39 or Y42 had a small effect, but the R17A/F39A and R17A/Y42A double mutants reduced efficiency 160- and 71-fold, respectively.

Re-examining the structure of *E. coli* OSBS revealed a similar cation−π interaction between R20 in the 20s loop and F51 in the 50s loop.[11] F51 is between the bound OSB and R20, which is at the surface of the protein and does not contact the ligand (Figure 4B). R20S and F51A mutations reduced efficiency 100- and 5-fold, respectively, and an R20S/F51A double mutant reduced efficiency nearly 500-fold.

As mentioned above, residues from the 20s and 50s loops of *T. fusca* OSBS, along with A229 and V230, form a hydrophobic pocket for binding the top of the cyclohexyl ring of the substrate (Figure 4B). Residues at structurally equivalent positions in *E. coli* OSBS (L19, L48, F51, S264, and I265) form a similar pocket. In both enzymes, single mutations at these positions tend to have little impact. It is only when we introduced mutations that disrupt interactions between the 20s and 50s loop that enzyme efficiency plummeted. Thus, the 20s and 50s loops interact in similar ways in *T. fusca* and *E. coli* OSBSs. This interaction is critical for forming the hydrophobic binding pocket, even though the identity of the hydrophobic amino acids in the pocket appears to be less important.

DISCUSSION

Analysis of structure−function relationships in *T. fusca* OSBS offers new insight into the structural diversity of the enolase superfamily. The most striking difference between *T. fusca* OSBS and most other structurally characterized members of the enolase superfamily is the site of substrate entry. In many enolase superfamily members, such as *E. coli* OSBS and *P. putida* mandelate racemase, the 20s loop is a flexible flap that assists catalysis by closing when ligand is bound.[11,14,27−30,37,38,42] In contrast, the 20s loop of *T. fusca* OSBS is ordered in the absence of both the substrate and metal ion, and it is truncated by four amino acids. Instead, the post-β5 loop becomes ordered when substrate binds. This side of the active site is blocked by other subunits in many multimeric enolase superfamily proteins.[2,13,30,33] *T. fusca* OSBS, however, is a monomer.

The only other known protein whose substrate enters from the 50s loop side of the active site is yeast enolase (PDB entry 1EBG).[37] In yeast enolase, the 20s loop is deleted, but this surface of the protein is the subunit interface of the homodimer. Instead, the 50s loop is extended, forming a flexible loop that closes the entrance to the active site.

The 20s loop is also truncated in several other members of the enolase superfamily. *Novosphingobium aromaticivorans* mannonate dehydratase (PDB entry 2QJN) and several uncharacterized members of the enolase superfamily (PDB entries 2GL5, 2QQ6, and 2OO6) compensate for the loss of the 20s loop with insertions after the first and/or second β-strands of the barrel domain.[33] As another variation on the theme, the truncated 20s loop of *Oceanobacillus iheyensis* galactarate dehydratase (PDB entry 3HPF) is compensated by a C-terminal extension that closes the active site when the ligand is bound.[2]

We also identified a cation−π interaction between the 20s and 50s loops that is important for forming a hydrophobic binding pocket in both *T. fusca* and *E. coli* OSBSs. This interaction is not conserved in the whole OSBS family. Some OSBSs lack aromatic residues in the 50s loop or basic residues in the part of the 20s loop that forms the hydrophobic binding pocket.[14] For example, the 20s loop of *Amycolatopsis* NSAR/OSBS interacts with the 50s loop only through hydrophobic interactions.[13] Instead, polar and basic residues in the 20s loop interact with the barrel domain, which would be too distant in *T. fusca* and *E. coli* OSBSs.

Finally, structural analysis and mutagenesis of *T. fusca* OSBS, *E. coli* OSBS, and *Amycolatopsis* NSAR/OSBS help to explain how proteins that have <30% amino acid sequence identity catalyze the same reaction. Sequences in the OSBS family diverged much more rapidly than those in other families in the enolase superfamily. For example, the average pairwise amino acid sequence identity of OSBSs from 66 species is 26%, while enolase enzymes from the same species average 56%.[7] Other work from our laboratory shows that this divergence correlates with a large number of deletions and a lack of quaternary structure in the OSBS family (D. Odokonyero et al., manuscript in preparation). Our results here show how this divergence is manifested in the active site. Ligand conformation differs between the NSAR/OSBS subfamily and other OSBS subfamilies.[11,13] Even though the ligand conformation is the same in *T. fusca* and *E. coli* OSBSs, different amino acids are important for binding and orienting the substrate for catalysis. Two amino acids were critical for activity in *E. coli* OSBS (R159 and G288), but mutation of the homologous residues in *T. fusca* OSBS (R128 and G254) had a modest effect. This could be due to stronger interactions with β-strand 1 of the barrel via hydrogen bonds in *T. fusca* OSBS. Alternatively, effects of these mutations might be masked by higher thermostability of *T. fusca* OSBS, which is from a thermophile.

A potential explanation for the rapid divergence of the OSBS family was that it is more tolerant of mutations than related families, possibly because of the lower energetic cost of aromatic ring formation in the OSBS reaction compared to the cost in other reactions initiated by abstracting a proton from the α-carbon adjacent to a carboxylate.[43] If this were true, many of the amino acid substitutions between *T. fusca* and *E. coli* OSBSs would be neutral. However, we discovered that mutating residues on β-strand 1 of the barrel in one protein to the amino acids found in the other protein reduced k_{cat}/K_M 33-fold in *T. fusca* OSBS and 385-fold in *E. coli* OSBS. Thus, although these mutations appear to be neutral when considering the overall reaction catalyzed by these enzymes, they do not have neutral effects on their molecular mechanisms. This incompatibility is probably due to subtle changes in the conformation and dynamics of the active site caused by amino acid substitutions at other positions. These results add support to an emerging theme in protein evolution, in which epistatic mutations (silent mutations that do not alter a protein's activity) place constraints on the amino acids that are permitted at other positions, making evolutionary pathways irreversible.[44,45]

dx.doi.org/10.1021/bi401176d | *Biochemistry* 2013, 52, 7512−7521

■ ASSOCIATED CONTENT

Supporting Information

Detailed methods, primers, and templates used for site-directed mutagenesis. This material is available free of charge via the Internet at http://pubs.acs.org.

■ AUTHOR INFORMATION

Corresponding Author

*Department of Biochemistry and Biophysics, Texas A&M University, 2128 TAMU, College Station, TX 77843-2128. E-mail: margy.glasner@tamu.edu. Phone: (979) 458-0123.

Funding

This work was supported by Grant A-1758 from the Robert A. Welch Foundation (Principle Investigator, M.E.G.). The NYSGXRC was supported by National Institutes of Health (NIH) Grant U54 GM074945 (Principal Investigator, S.K.B.). The NYSGRC is supported by NIH Grant U54 GM094662 (Principal Investigator, S.C.A.). The Center for Synchrotron Biosciences, where diffraction data were collected, was supported by Grant P30-EB-009998 from the National Institute of Biomedical Imaging and Bioengineering. Use of the National Synchrotron Light Source, Brookhaven National Laboratory, was supported by the U.S. Department of Energy, Office of Science, Office of Basic Energy Sciences, under Contract DE-AC02-98CH10886.

Notes

The authors declare no competing financial interest.

■ ACKNOWLEDGMENTS

We acknowledge the efforts of all NYSGXRC and NYSGRC personnel who contributed to the structure determination and manuscript preparation. We thank Chenxi Wang, Wan Wen Zhu, and Christine Jones for assistance with site-directed mutagenesis and Dr. Andrew McMillan for insightful comments on the manuscript.

■ ABBREVIATIONS

OSBS, *o*-succinylbenzoate synthase; NSAR, *N*-succinylamino acid racemase; SHCHC, 2-succinyl-6-hydroxy-2,4-cyclohexadiene-1-carboxylate; PMSF, phenylmethanesulfonyl fluoride; PDB, Protein Data Bank.

■ REFERENCES

(1) Gerlt, J. A., Babbitt, P. C., and Rayment, I. (2005) Divergent evolution in the enolase superfamily: The interplay of mechanism and specificity. *Arch. Biochem. Biophys. 433*, 59−70.

(2) Rakus, J. F., Kalyanaraman, C., Fedorov, A. A., Fedorov, E. V., Mills-Groninger, F. P., Toro, R., Bonanno, J., Bain, K., Sauder, J. M., Burley, S. K., Almo, S. C., Jacobson, M. P., and Gerlt, J. A. (2009) Computation-facilitated assignment of the function in the enolase superfamily: A regiochemically distinct galactarate dehydratase from *Oceanobacillus iheyensis*. *Biochemistry 48*, 11546−11558.

(3) Song, L., Kalyanaraman, C., Fedorov, A. A., Fedorov, E. V., Glasner, M. E., Brown, S., Imker, H. J., Babbitt, P. C., Almo, S. C., Jacobson, M. P., and Gerlt, J. A. (2007) Prediction and assignment of function for a divergent *N*-succinyl amino acid racemase. *Nat. Chem. Biol. 3*, 486−491.

(4) Kalyanaraman, C., Imker, H. J., Fedorov, A. A., Fedorov, E. V., Glasner, M. E., Babbitt, P. C., Almo, S. C., Gerlt, J. A., and Jacobson, M. P. (2008) Discovery of a dipeptide epimerase enzymatic function guided by homology modeling and virtual screening. *Structure 16*, 1668−1677.

(5) Lukk, T., Sakai, A., Kalyanaraman, C., Brown, S. D., Imker, H. J., Song, L., Fedorov, A. A., Fedorov, E. V., Toro, R., Hillerich, B., Seidel, R., Patskovsky, Y., Vetting, M. W., Nair, S. K., Babbitt, P. C., Almo, S. C., Gerlt, J. A., and Jacobson, M. P. (2012) Homology models guide discovery of diverse enzyme specificities among dipeptide epimerases in the enolase superfamily. *Proc. Natl. Acad. Sci. U.S.A. 109*, 4122−4127.

(6) Meganathan, R. (2001) Biosynthesis of menaquinone (vitamin K_2) and ubiquinone (coenzyme Q): A perspective on enzymatic mechanisms. *Vitam. Horm. 61*, 173−218.

(7) Glasner, M. E., Fayazmanesh, N., Chiang, R. A., Sakai, A., Jacobson, M. P., Gerlt, J. A., and Babbitt, P. C. (2006) Evolution of structure and function in the *o*-succinylbenzoate synthase/*N*-acylamino acid racemase family of the enolase superfamily. *J. Mol. Biol. 360*, 228−250.

(8) Sakai, A., Xiang, D. F., Xu, C., Song, L., Yew, W. S., Raushel, F. M., and Gerlt, J. A. (2006) Evolution of enzymatic activities in the enolase superfamily: *N*-Succinylamino acid racemase and a new pathway for the irreversible conversion of D- to L-Amino Acids. *Biochemistry 45*, 4455−4462.

(9) Palmer, D. R., Garrett, J. B., Sharma, V., Meganathan, R., Babbitt, P. C., and Gerlt, J. A. (1999) Unexpected divergence of enzyme function and sequence: "*N*-Acylamino acid racemase" is *o*-succinylbenzoate synthase. *Biochemistry 38*, 4252−4258.

(10) Taylor Ringia, E. A., Garrett, J. B., Thoden, J. B., Holden, H. M., Rayment, I., and Gerlt, J. A. (2004) Evolution of enzymatic activity in the enolase superfamily: Functional studies of the promiscuous *o*-succinylbenzoate synthase from *Amycolatopsis*. *Biochemistry 43*, 224−229.

(11) Thompson, T. B., Garrett, J. B., Taylor, E. A., Meganathan, R., Gerlt, J. A., and Rayment, I. (2000) Evolution of enzymatic activity in the enolase superfamily: Structure of *o*-succinylbenzoate synthase from *Escherichia coli* in complex with Mg^{2+} and *o*-succinylbenzoate. *Biochemistry 39*, 10662−10676.

(12) Klenchin, V. A., Taylor Ringia, E. A., Gerlt, J. A., and Rayment, I. (2003) Evolution of enzymatic activity in the enolase superfamily: Structural and mutagenic studies of the mechanism of the reaction catalyzed by *o*-succinylbenzoate synthase from *Escherichia coli*. *Biochemistry 42*, 14427−14433.

(13) Thoden, J. B., Taylor Ringia, E. A., Garrett, J. B., Gerlt, J. A., Holden, H. M., and Rayment, I. (2004) Evolution of enzymatic activity in the enolase superfamily: Structural studies of the promiscuous *o*-succinylbenzoate synthase from *Amycolatopsis*. *Biochemistry 43*, 5716−5727.

(14) Zhu, W. W., Wang, C., Jipp, J., Ferguson, L., Lucas, S. N., Hicks, M. A., and Glasner, M. E. (2012) Residues required for activity in *Escherichia coli o*-succinylbenzoate synthase (OSBS) are not conserved in all OSBS enzymes. *Biochemistry 51*, 6171−6181.

(15) Rost, B. (2002) Enzyme function less conserved than anticipated. *J. Mol. Biol. 318*, 595−608.

(16) Tian, W., and Skolnick, J. (2003) How well is enzyme function conserved as a function of pairwise sequence identity? *J. Mol. Biol. 333*, 863−882.

(17) Sauder, M. J., Rutter, M. E., Bain, K., Rooney, I., Gheyi, T., Atwell, S., Thompson, D. A., Emtage, S., and Burley, S. K. (2008) High throughput protein production and crystallization at NYSGXRC. *Methods Mol. Biol. 426*, 561−575.

(18) Sheldrick, G. M. (2008) A short history of SHELX. *Acta Crystallogr. A64*, 112−122.

(19) Bricogne, G., Vonrhein, C., Flensburg, C., Schiltz, M., and Paciorek, W. (2003) Generation, representation and flow of phase information in structure determination: Recent developments in and around SHARP 2.0. *Acta Crystallogr. D59*, 2023−2030.

(20) Abrahams, J. P., and Leslie, A. G. (1996) Methods used in the structure determination of bovine mitochondrial F1 ATPase. *Acta Crystallogr. D52*, 30−42.

(21) Collaborative Computational Project, No. 4 (1994) The CCP4 suite: Programs for protein crystallography. *Acta Crystallogr. D50*, 760−763.

(22) Emsley, P., and Cowtan, K. (2004) Coot: Model-building tools for molecular graphics. *Acta Crystallogr. D60*, 2126−2132.

(23) Brunger, A. T., Adams, P. D., Clore, G. M., DeLano, W. L., Gros, P., Grosse-Kunstleve, R. W., Jiang, J. S., Kuszewski, J., Nilges, M., Pannu, N. S., Read, R. J., Rice, L. M., Simonson, T., and Warren, G. L. (1998) Crystallography & NMR system: A new software suite for macromolecular structure determination. *Acta Crystallogr. D54*, 905–921.
(24) Vagin, A., and Teplyakov, A. (1997) MOLREP: An Automated Program for Molecular Replacement. *J. Appl. Crystallogr. 30*, 1022–1025.
(25) Pettersen, E. F., Goddard, T. D., Huang, C. C., Couch, G. S., Greenblatt, D. M., Meng, E. C., and Ferrin, T. E. (2004) UCSF Chimera: A visualization system for exploratory research and analysis. *J. Comput. Chem. 25*, 1605–1612.
(26) Wang, W., and Malcolm, B. A. (1999) Two-stage PCR protocol allowing introduction of multiple mutations, deletions and insertions using QuikChange site-directed mutagenesis. *BioTechniques 26*, 680–682.
(27) Neidhart, D. J., Howell, P. L., Petsko, G. A., Powers, V. M., Li, R. S., Kenyon, G. L., and Gerlt, J. A. (1991) Mechanism of the reaction catalyzed by mandelate racemase. 2. Crystal structure of mandelate racemase at 2.5-Å resolution: Identification of the active site and possible catalytic residues. *Biochemistry 30*, 9264–9273.
(28) Landro, J. A., Gerlt, J. A., Kozarich, J. W., Koo, C. W., Shah, V. J., Kenyon, G. L., Neidhart, D. J., Fujita, S., and Petsko, G. A. (1994) The role of lysine 166 in the mechanism of mandelate racemase from *Pseudomonas putida*: Mechanistic and crystallographic evidence for stereospecific alkylation by (R)-α-phenylglycidate. *Biochemistry 33*, 635–643.
(29) Gulick, A. M., Hubbard, B. K., Gerlt, J. A., and Rayment, I. (2000) Evolution of enzymatic activities in the enolase superfamily: Crystallographic and mutagenesis studies of the reaction catalyzed by D-glucarate dehydratase from *Escherichia coli*. *Biochemistry 39*, 4590–4602.
(30) Klenchin, V. A., Schmidt, D. M., Gerlt, J. A., and Rayment, I. (2004) Evolution of enzymatic activities in the enolase superfamily: Structure of a substrate-liganded complex of the L-Ala-D/L-Glu epimerase from *Bacillus subtilis*. *Biochemistry 43*, 10370–10378.
(31) Yew, W. S., Fedorov, A. A., Fedorov, E. V., Rakus, J. F., Pierce, R. W., Almo, S. C., and Gerlt, J. A. (2006) Evolution of enzymatic activities in the enolase superfamily: L-Fuconate dehydratase from *Xanthomonas campestris*. *Biochemistry 45*, 14582–14597.
(32) Yew, W. S., Fedorov, A. A., Fedorov, E. V., Wood, B. M., Almo, S. C., and Gerlt, J. A. (2006) Evolution of enzymatic activities in the enolase superfamily: D-Tartrate dehydratase from *Bradyrhizobium japonicum*. *Biochemistry 45*, 14598–14608.
(33) Rakus, J. F., Fedorov, A. A., Fedorov, E. V., Glasner, M. E., Vick, J. E., Babbitt, P. C., Almo, S. C., and Gerlt, J. A. (2007) Evolution of enzymatic activities in the enolase superfamily: D-Mannonate dehydratase from *Novosphingobium aromaticivorans*. *Biochemistry 46*, 12896–12908.
(34) Rakus, J. F., Fedorov, A. A., Fedorov, E. V., Glasner, M. E., Hubbard, B. K., Delli, J. D., Babbitt, P. C., Almo, S. C., and Gerlt, J. A. (2008) Evolution of enzymatic activities in the enolase superfamily: L-Rhamnonate dehydratase. *Biochemistry 47*, 9944–9954.
(35) Sakai, A., Fedorov, A. A., Fedorov, E. V., Schnoes, A. M., Glasner, M. E., Brown, S., Rutter, M. E., Bain, K., Chang, S., Gheyi, T., Sauder, J. M., Burley, S. K., Babbitt, P. C., Almo, S. C., and Gerlt, J. A. (2009) Evolution of enzymatic activities in the enolase superfamily: Stereochemically distinct mechanisms in two families of *cis,cis*-muconate lactonizing enzymes. *Biochemistry 48*, 1445–1453.
(36) Lietzan, A. D., Nagar, M., Pellmann, E. A., Bourque, J. R., Bearne, S. L., and St Maurice, M. (2012) Structure of mandelate racemase with bound intermediate analogues benzohydroxamate and Cupferron. *Biochemistry 51*, 1160–1170.
(37) Wedekind, J. E., Poyner, R. R., Reed, G. H., and Rayment, I. (1994) Chelation of serine 39 to Mg^{2+} latches a gate at the active site of enolase: structure of the bis(Mg^{2+}) complex of yeast enolase and the intermediate analog phosphonoacetohydroxamate at 2.1-Å resolution. *Biochemistry 33*, 9333–9342.
(38) Bourque, J. R., and Bearne, S. L. (2008) Mutational analysis of the active site flap (20s loop) of mandelate racemase. *Biochemistry 47*, 566–578.
(39) Sugawara, T., Kuwajima, K., and Sugai, S. (1991) Folding of Staphylococcal Nuclease A Studied by Equilibrium and Kinetic Circular-Dichroism Spectra. *Biochemistry 30*, 2698–2706.
(40) Berka, K., Anzenbacherova, E., Hendrychova, T., Lange, R., Masek, V., Anzenbacher, P., and Otyepka, M. (2012) Binding of quinidine radically increases the stability and decreases the flexibility of the cytochrome P450 2D6 active site. *J. Inorg. Biochem. 110*, 46–50.
(41) Dundas, J., Ouyang, Z., Tseng, J., Binkowski, A., Turpaz, Y., and Liang, J. (2006) CASTp: Computed atlas of surface topography of proteins with structural and topographical mapping of functionally annotated residues. *Nucleic Acids Res. 34*, W116–W118.
(42) Lebioda, L., and Stec, B. (1988) Crystal structure of enolase indicates that enolase and pyruvate kinase evolved from a common ancestor. *Nature 333*, 683–686.
(43) Taylor, E. A., Palmer, D. R., and Gerlt, J. A. (2001) The lesser "burden borne" by *o*-succinylbenzoate synthase: An "easy" reaction involving a carboxylate carbon acid. *J. Am. Chem. Soc. 123*, 5824–5825.
(44) Bridgham, J. T., Ortlund, E. A., and Thornton, J. W. (2009) An epistatic ratchet constrains the direction of glucocorticoid receptor evolution. *Nature 461*, 515–519.
(45) Gong, L. I., Suchard, M. A., and Bloom, J. D. (2013) Stability-mediated epistasis constrains the evolution of an influenza protein. *eLife 2*, e00631.